J Mater Sci (2013) 48:2920–2927
DOI 10.1007/s10853-012-6923-z

Study of the microstructure of inkjet-printed P3HT:PCBM blend for photovoltaic applications

Pasquale Morvillo · Immacolata Angelica Grimaldi · Rosita Diana · Fausta Loffredo · Fulvia Villani

Received: 22 May 2012 / Accepted: 27 September 2012 / Published online: 16 October 2012

Abstract Recently, great interest has been devoted to cost-effective alternative energy sources such as organic solar cells because of the mechanical flexibility and the versatility of chemical structure, the low cost of fabrication, and ease of processing. As regards this last point, the possibility to deposit organic materials from solutions at low temperatures makes them employable for fabricating printed solar cells by direct printing methods. In this study, we used the inkjet-printing technology to deposit P3HT blends with various fullerene acceptors ([60]PCBM, [70]PCBM and bis[60]PCBM) dissolved in single solvents, 1,2-dichlorobenzene (DCB) and chlorobenzene (CB), and their mixtures. After optimizing the printing parameters (printhead speed, drop emission frequency, and substrate temperature), the effect of the solvents on the morphology of the photoactive layers was analyzed through Raman spectroscopy and atomic force microscopy. Polymer solar cells with the structure glass/ITO/PEDOT:PSS/blend/Ca/Al were fabricated and characterized by current–voltage (I–V) measurements under 100 mW/cm^2 AM 1.5G illumination. A comparative study of the performances of the devices was performed based on three different fullerene derivatives, correlating them to the microstructure of the printed blend films. The optimal devices were obtained when the blend films were deposited from a mixture of DCB:CB 4:1 by volume: this was in agreement with the most favorable morphology of these films.

P. Morvillo (✉) · I. A. Grimaldi · R. Diana · F. Loffredo · F. Villani
ENEA, C.R. Portici, UTTP-NANO, Piazzale Enrico Fermi 1, 80055 Portici, Naples, Italy
e-mail: pasquale.morvillo@enea.it

I. A. Grimaldi
Department of Physics Science, University of Naples Federico II, Piazzale Tecchio, 80125 Naples, Italy

Introduction

During the recent decades, there has been an intensive effort to develop organic photovoltaics as cost-effective renewable energy sources opening the route to new applications, such as self-powered electronic systems or self-sufficient buildings. The potential advantages of organic solar cells over the inorganic ones are their mechanical flexibility and the expected low processing cost for large-area scale using environment-friendly techniques [1–4].

The main factors that promoted the rapid development of this technology were the synthesis of new materials, the definition of appropriate architectures and the introduction of innovative processing techniques [3]. Concerning the materials, the growing number of conjugated polymers and molecules with high optical absorption coefficient in the visible range of the solar radiation [5] offered an inexpensive alternative to the inorganic semiconductors and the possibility for the production of very thin solar cells. Moreover, as the light absorption for this class of materials results in the formation of a mobile excited state (exciton) and the exciton diffusion lengths are typically 1–10 nm [6–8], the study of efficient structures that allow us to minimize significant recombination losses has been another crucial issue. Currently, bulk heterojunction (BHJ) configuration for the photoactive layer, where the donor and acceptor components are blended together so that their intimate mix creates donor–acceptor interfaces within smaller distances than the exciton diffusion length, is the most acclaimed architecture for assuring an efficient charge transfer in polymer solar cells (PSCs) [9–11].

In addition, the solubility of this class of materials in common organic solvents makes the PSCs particularly attractive as thin flexible devices can be manufactured through high-throughput, low-temperature processes that employ printing methodologies in roll-to-roll (R2R) configuration [12], such as slot-die coating and screen printing [13, 14], gravure [15], and inkjet printing (IJP) [3, 16–20]. Actually, there are several examples in the literature of self-powered systems using PSCs, such as the organic photovoltaic-powered electrochromic displays [21], the small credit card-sized lamp with a flat outline (integrated into the Organic Electronics Association demonstrator in the year 2011) [22], and the lamp for the ''Lighting Africa'' initiative [23]. So far, the most successful R2R techniques for the realization of PSCs have been slot-die coating for the active layer and screen printing for electrodes [14]. These techniques employ complex and expensive masters for the definition of the two-dimensional patterning and use large quantity of materials with remarkable wastes. Conversely, IJP employs very minute amounts of materials, deposits selectively, and patterns them at the same time under no-contact and no-vacuum conditions by means of digital masters realized with CAD software, thereby guarantying high precision and accuracy in the deposition process. All these features make IJP a promising technique for PSC processing, although until now it has not been largely tested in R2R configuration [12].

The quality of inkjet-printed layers and their morphologies are strongly influenced by the ink composition (nature of the solvents, concentration of active materials, etc.) and printing parameters. In general, the droplet drying process is dominated by the "coffee-stain" effect that provokes an inhomogeneity of the printed film [24]. This effect can be suitably balanced inducing a Marangoni flow by means of solvent mixtures, namely, controlling the ink's chemico-physical properties [25–27]. In this way, the uniformity can be improved by driving the solute diffusion inside the sessile drop in a controlled manner. This phenomenon is common and takes place with various functional materials, also for other applications [28], but is a crucial aspect in the PSCs. Indeed, the transport of electrons/holes in the BHJ devices is very sensitive to the morphology of the blend. Therefore, in general, the control of the photoactive layer morphology has a strong impact on the performances of the PSCs and remains a particularly critical issue in printed devices.

Although several studies demonstrated how the solvent for dissolving the polymer and its concentration in solution have a significant influence on the morphology as well as the solvent mixture-based approach has a key role on organic solar cell performances [17, 19, 20, 29–31], many aspects related to the microstructure, particularly the one of printed photoactive layers, and its correlation to the device performances, nevertheless remain to be investigated further.

The most exploited active blend for PSCs is based on a BHJ of poly(3-hexylthiophene) (P3HT) (donor material) and [6]-phenyl C_{61}-butyric acid methyl ester ([60]PCBM) (acceptor material): using this material, a power conversion efficiency (PCE) of 5 % has been reached [9]. Nevertheless, recently, other fullerene derivatives have been prepared and used as electron acceptors for PSCs in conjunction with P3HT producing better performances (up to 7 %) in the corresponding devices [32–36]. These enhancements are mainly due to improvements of the short-circuit current density (J_{sc}) and the open-circuit voltage (V_{oc}).

In this study, we made inkjet-printed blends of P3HT with various fullerene acceptors, [60]PCBM, [6]-phenyl-C_{71}-butyric acid methyl ester ([70]PCBM), and bis(1-[3-(methoxycarbonyl)propyl]-1-phenyl)-[6.6]C_{62} (bis[60]PCBM), dissolved in single solvents, 1,2-dichlorobenzene (DCB), and chlorobenzene (CB), and their mixtures. After optimizing the printing parameters (printhead speed, drop emission frequency, and substrate temperature), the effect of the solvents on the morphology of the layers was analyzed through Raman spectroscopy and atomic force microscopy (AFM). PSCs with structure glass/indium tin oxide (ITO)/poly(3,4-ethylenedioxythiophene):poly(styrenesulfonate) (PEDOT:PSS)/blend/Ca/Al were fabricated and characterized by current–voltage (I–V) measurements under 100 mW/cm^2 AM 1.5G illumination. The performances of the devices were analyzed and correlated to the microstructure of the blend film.

Experimental

Materials and preparation of inks

Three fullerenes, [60]PCBM, [70]PCBM, and bis[60]PCBM, were employed as acceptors to prepare different BHJ blend materials in conjunction with P3HT. Regioregular P3HT (Plextronics) and [60]PCBM, [70]PCBM, and bis[60]PCBM (Solenne BV) were used as received. The blends were prepared by employing P3HT (6.0 mg/mL) and [60]PCBM (4.8 mg/mL) or [70]PCBM (4.8 mg/mL) or bis[60]PCBM (6.0 mg/mL) with mixing ratio of 1:0.8, 1:0.8, or 1:1 by weight, respectively. Different blend inks were obtained by dissolving each donor/acceptor system in two different single solvents, DCB ($T_b = 180$ °C, $\gamma = 26.84$ mN/m) and CB ($T_b = 131$ °C, $\gamma = 33.4$ mN/m), and in DCB:CB mixtures at volume mixing ratios of 4:1, 1:1, 1:4. All the solutions were stirred on hotplate at 50 °C for 24 h before printing.

An aqueous solution of PEDOT:PSS (Clevios P Al 4083) was used as hole-conducting material.

ITO-coated glass substrates (Corning® Eagle 2000) with sheet resistance lower than 15 Ω/□ were purchased from Delta Technologies, LTD.

Printing of active layers

The three different active materials were deposited onto the hole transport layer (PEDOT:PSS) by the IJP technology. The prints were carried out by means of an equipment (Aurel S.p.A.) which uses a piezoelectric Drop on Demand (DoD) Microdrop printhead (30-μm opening nozzle, and 20-pL droplet volume). The system allows us to control the temperature of the substrate, both flexible, reel or single sheet, and nonflexible one, ranging from T_{amb} to 100 °C.

The substrate temperature was optimized for each ink to prevent the coalescence of the droplets printed on the target substrate. Specifically, the substrate temperatures were 22 °C for CB, 60 °C for both DCB and DCB:CB 4:1, and 40 °C for DCB:CB 1:1 and 1:4.

Active material films were deposited by printing sequences of overlapped droplets with 50 % overlapping degree, 15 Hz drop emission frequency, and 1.2 mm/s printhead speed. These printing parameters, including the substrate temperature, were selected after an optimization process performed for each investigated solvent composition with the aim of reaching the best film uniformity condition. The active layer thickness ranged between 130 and 160 nm for all the investigated blends.

The IJP process was carried out in environmental condition, at room temperature.

PSCs realization

The devices were manufactured with BHJ configuration, where the active layer was sandwiched between two electrodes with different work functions. The ITO-coated glass substrates were first cleaned with detergent, then, ultrasonicated in acetone and isopropanol, and subsequently dried in oven. After a selective etching of a part of the ITO to define the geometry of the front electrode, films of PEDOT:PSS were spin coated at 5000 rpm for 60 s after passing through a 0.45-μm filter. The thickness of the PEDOT:PSS layer was 30 nm. The samples were dried for 60 min at 140 °C in air. The active materials were printed on top of hole transporting layer by realizing surfaces of 96 mm^2. This area was enough for completely covering the area of the bottom ITO electrode. After printing, the active films were dried under nitrogen flow at 100 °C for 1 h. On top of photoactive layer, the Ca electrode (20 nm) capped with Al (80 nm) was deposited by thermal evaporation in ultra-high vacuum (10^{-7} mbar) using a shadow mask to define the active area of the device (35 mm^2). Finally, a thermal annealing was carried out by taking the samples on hotplate at 150 °C for 30 min in a nitrogen-filled glow box.

Characterizations

The thickness of the films was measured by means of a surface profilometer (KLA Tencor P-10 Surface Profiler). Raman spectroscopy was performed through a Renishaw InVia Reflex Raman spectrometer using a 514.5-nm excitation source. The surface morphology of the inkjet-printed BHJ polymer–fullerene blend layers was analyzed by atomic force microscopy (AFM, Veeco, Dimension Digital Instruments Nanoscope IV) in tapping mode. All the PSCs were characterized in air at room temperature (∼25 °C) and without encapsulation by means of current–voltage (I–V) measurements performed under simulated light. I–V light characteristic was measured using a Keithley 236 source measure unit (Keithley Instruments Inc., Cleveland, USA). The voltage ramp rate, controlled by a PC program, was of 10 mV/s from positive-to-negative potential. Simulated AM 1.5G white light illumination was provided by a class "AAA" Wacom Solar Simulator, Model WXS155S, equipped with two lamps (Xenon and Halogen), and its intensity was calibrated using an unfiltered mono-Si reference cell (certified by ESTI) for 1 sunlight intensity of 100 mW/cm^2.

Results and discussion

As the morphology of the photoactive layer strongly affects the performances of the BHJ device consisting of a phase-separated mix of acceptor and donor components and as in inkjet-printing processing, similar to solution deposition method, both phase separation and molecular self-organization are significantly controlled by the solvent evaporation, the study of the effects of the solvent composition on the morphology is aimed to determine key elements to enhance the organic solar cells. In this respect, the morphology of the P3HT in blends with different fullerene derivatives dissolved in pure solvents and in solvent mixtures was investigated by means of Raman spectroscopy in the frequency range 1000–2000 cm^{-1} by means of a 514-nm laser excitation. All the prepared photoactive films showed a common spectrum shape characterized by the presence of two main bands, the typical ones associated to the vibrational frequencies of P3HT polymer chain. In Fig. 1, the Raman spectra of inkjet-printed P3HT:[60]PCBM, P3HT:[70]PCBM, P3HT:bis[60]PCBM films by chlorobenzene solution are reported as example. The band observed at 1375–1380 cm^{-1} is associated to Cβ–Cβ skeletal stretching in the aromatic thiophene ring, whereas the strong intensity band centered at 1445–1455 cm^{-1} is related to Cα=Cβ stretching of the aromatic thiophene ring [37–40]. Both these peaks are sensitive to π-electron delocalization, namely, the conjugation length, of P3HT molecules [41]. In particular, the quantitative analysis (peak position and full width at half maximum (FWHM)) of the peak at 1445–1455 cm^{-1} can give information about the homogeneity and molecular

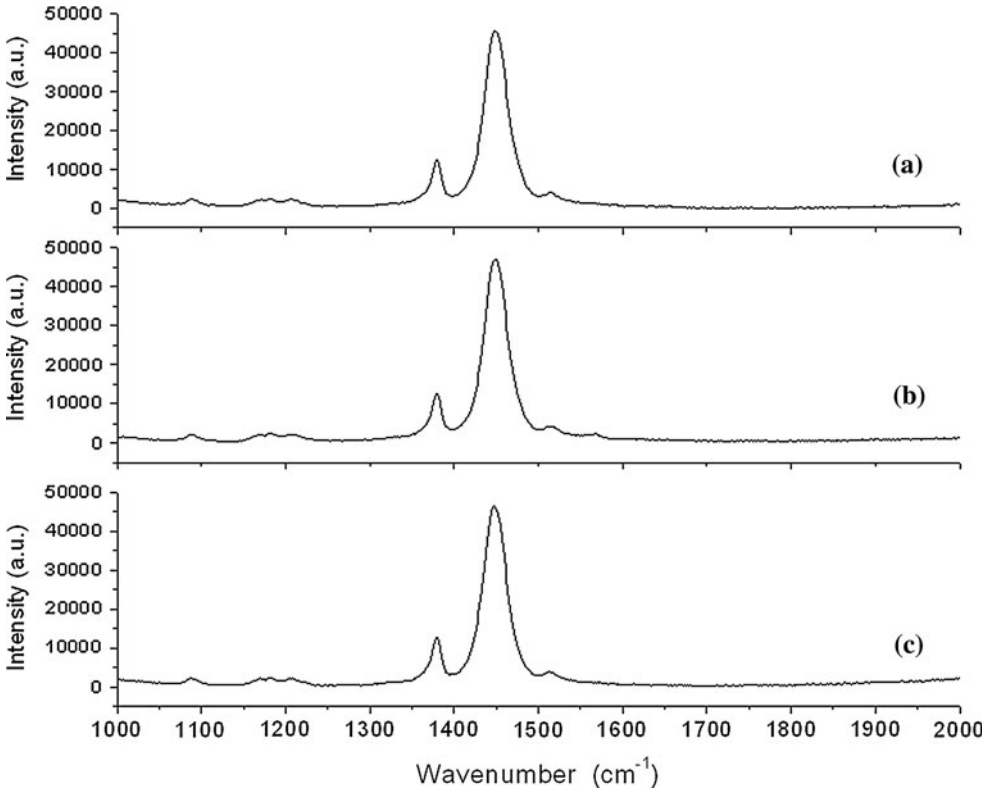

Fig. 1 Raman spectra under 514 nm excitation of **a** P3HT:[60]PCBM, **b** P3HT:[70]PCBM, **c** P3HT:bis[60]PCBM blend films deposited by inkjet printing of chlorobenzene solutions

order of P3HT chains in the film which are correlated to the crystallinity in P3HT phase [40, 41]. Specifically, the increased crystallite size and the better internal order within P3HT domains leads to narrowing and weakening in the symmetrical stretching.

Therefore, to evaluate the effect of solvents and solvent mixtures on the film morphology, the Raman peak at 1445–1455 cm^{-1} for the films obtained by dissolving the blends in pure CB, pure DCB, and DCB:CB mixtures at different DCB volume fractions (X_{DCB}: 0.2, 0.5, 0.8) was analyzed. The results showed that the Raman shift of the Cα=Cβ peak remained almost constant, but variations of the peak FWHM were observed. FWHM of Cα=Cβ symmetric stretching peak of Raman spectrum was evaluated by fitting each curve with a Lorentzian function: the estimated values for all the investigated samples are reported in Fig. 2. In detail, this analysis showed that the employment of the solvent mixture reduces the peak FWHM indicating an extension of the conjugation length along the polymer backbone. For each used fullerene derivative, the minimum value of the peak FWHM was obtained for the $X_{DCB} = 0.8$. This means that the DCB:CB mixture at volume mixing ratio 4:1 induces a reduced disorder in P3HT:PCBM blend that can be correlated to a higher stacking of conjugated P3HT segment and a segregation of PCBM into PCBM-rich regions. This effect could be attributed to a more uniform evaporation rate of the solvent

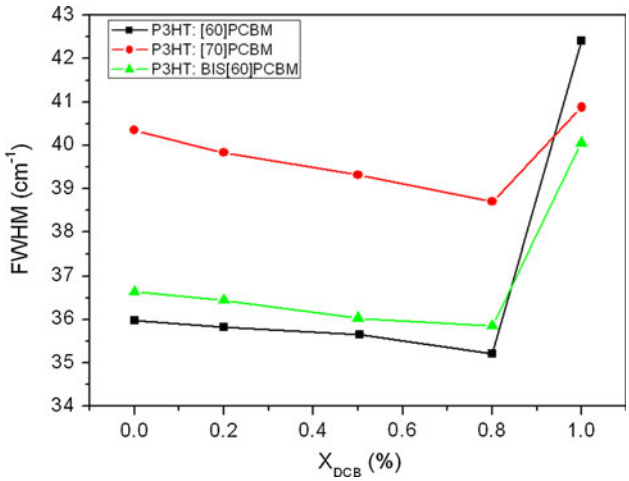

Fig. 2 Full width at half maximum (FWHM)) of 1445 cm^{-1} peak of raman spectra of P3HT:[60]PCBM (*square*), P3HT:[70]PCBM (*circle*) and P3HT:bis[60]PCBM (*triangle*) films obtained by inks with different dichlorobenzene (DCB) volume fractions

mixture with respect to pure solvent, which leads to a better homogeneity in the chain conformation in the amorphous portion of P3HT with a higher degree of phase separation between P3HT and PCBM.

On the basis of these results, to further investigate the solvent role in blend processing and its effect on the microstructure of the printed photoactive layer, the

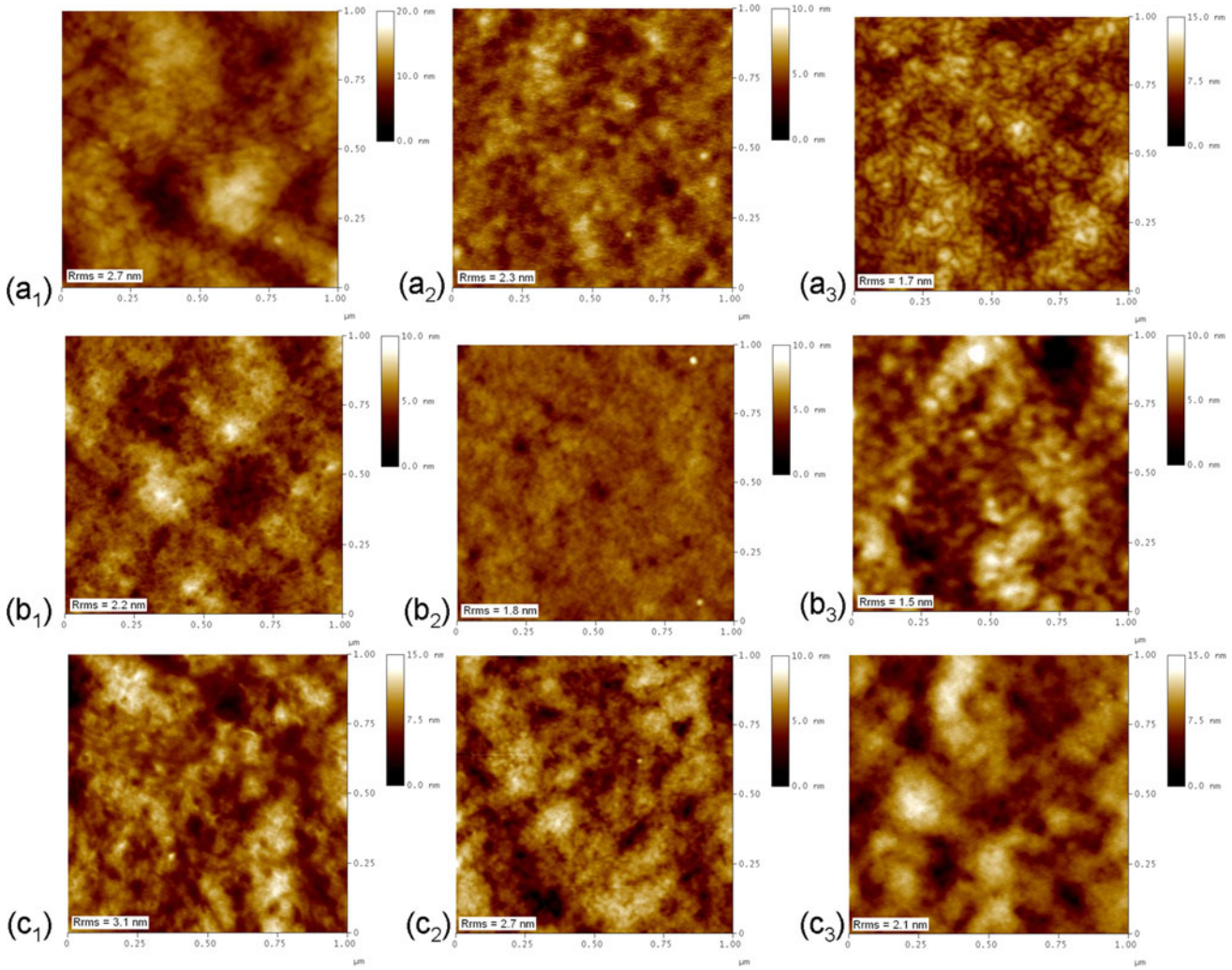

Fig. 3 AFM topographic images (scan size $1 \times 1\ \mu m^2$) of inkjet-printed ($\mathbf{a_x}$) P3HT:[60]PCBM, ($\mathbf{b_x}$) P3HT:[70]PCBM and ($\mathbf{c_x}$) P3HT:bis[60]PCBM blend films starting from CB ($\mathbf{a_1}$, $\mathbf{b_1}$, $\mathbf{c_1}$), DCB ($\mathbf{a_2}$, $\mathbf{b_2}$, $\mathbf{c_2}$), and DCB:CB 4:1 ($\mathbf{a_3}$, $\mathbf{b_3}$, $\mathbf{c_3}$) solutions

morphology of the prepared film surfaces was analyzed also by AFM.

Morphologic analysis of all the films prepared using the various P3HT:fullerene blends, each one by means of solvent mixtures at different volume mixing ratios, indicated a good intermixing of the polymer and fullerene components, characterized by uniform surfaces with root-mean-square-roughness (R_{rms}) values of around 1–3 nm. Therefore, taking into account also the indications obtained from Raman analysis, in Fig. 3 are reported the AFM topographic images of the surfaces of the samples prepared with the different fullerene derivatives with the solvent mixture DCB:CB 4:1 and, as reference, those ones with the pure solvents. The effect of the solvent composition on the film morphology showed a common behavior for the three fullerene-based blends: for each fullerene derivative, a slight increase of R_{rms} value was detected for the pure-solvent systems, in particular, the highest one was registered for CB. This can be attributed to the high evaporation rate of the CB, having lower boiling point, and higher vapor pressure, which makes the drying process faster, thus not promoting the self-organization of the blended polymer molecules. Anyway, the smooth roughness observed for all the samples acts as the index endorsing that the phase separation between P3HT and fullerene derivatives has occurred [31]. In confirmation of this, no large domains were observed from the images, but only few small nanoclusters with average dimension of about 10–20 nm and with clear edges, differentiating themselves from the surrounding phase. Only the sample prepared with P3HT:[60]PCBM from solvent mixture DCB:CB 4:1 showed nicely defined features highlighting a different phase segregation induced by this specific solvent system though its surface roughness being low anyway ($R_{rms} = 1.7$ nm).

In order to study how the morphology of printed blend layers affects the charge transport in organic solar cells and, hence, their performances, P3HT:[60]PCBM, P3HT:[70]PCBM and

P3HT:bis[60]PCBM blend films, dissolved in single solvents and their mixtures, were inserted as photoactive materials in BHJ structures. The stack of the device was glass/ITO/PEDOT:PSS/blend/Ca/Al.

The V_{oc}, J_{sc}, fill factor (FF), and PCEs of all the devices, characterized by I–V measurements performed under simulated AM 1.5G illumination (100 mW/cm^2), are summarized in Table 1. In Fig. 4, the PCEs of the solar cells based on the three blend films as a function of the solvent mixture composition are reported. The performances of the devices with the three kinds of acceptors increase with the content of DCB reaching a maximum when the blend films are dissolved in the DCB:CB 4:1 solution. The PCE reaches the values of 2.22, 1.24, and 0.74 % for the device based on the blend film of P3HT:[60]PCBM, P3HT:[70]PCBM and P3HT:bis[60]PCBM, respectively. This result can be correlated to the indications coming from morphologic analyses. Indeed, the Raman spectroscopy indicated that the use of the solvent mixture DCB:CB 4:1 improves the homogeneity in the chain conformation in the amorphous portion of P3HT and increases the degree of phase separation between P3HT and PCBM. In addition, the same samples had very uniform surfaces with the lowest R_{rms} values and, in particular, the one based on the [60]PCBM acceptor produced a different phase segregation in comparison with the others. This can be explained in terms of the chemicophysical properties of the inks. Both P3HT and the used fullerene derivatives are well soluble in chlorinated solvents like DCB an CB [42]. Unfortunately, CB has a lower boiling point with respect to DCB, and so inducing a fast evaporation during the droplet drying and, hence, a non-optimized blend morphology. On the other hand, DCB generates a bad spreading and wetting of the blend ink on the hole-conducting underlayer as already reported in studies on analogs [16]. The use of solvent mixtures, in particular DCB:CB 4:1, enhances the wetting of the photoactive material on the substrate assuring the intimate morphology within the blend.

The electrical analysis showed a lower J_{sc} for the devices based on the P3HT:[70]PCBM blend compared with the P3HT:[60]PCBM ones (except the PSCs realized from CB solvent), although [70]PCBM has a stronger and broader absorption compared with [60]PCBM, and it should partially compensate the limited absorption of the donor polymer in the visible region of the spectrum, thus improving the output current of the corresponding polymer–fullerene devices [34, 35]. On the other hand, electrical losses arising from the "coffee-stain" effect can have different impact on different materials limiting the output current of the corresponding devices.

The V_{oc} of all the devices (except those realized using blend films dissolved in pure DCB) are very close to the state-of-the-art of the corresponding ones in which the photoactive material is prepared by spin coating.

Furthermore, P3HT:bis[60]PCBM was characterized by an higher V_{oc} with respect the devices based on the other fullerene derivative blends. Indeed, the V_{oc} of a BHJ PSCs, within certain limits [43–46], is related to the difference between the highest occupied molecular orbital (HOMO) of the electron donor and the lowest unoccupied molecular orbital (LUMO) of the electron acceptor [43, 44], although

Table 1 Photovoltaic properties (under illumination of AM 1.5G, 100 mW/cm^2) of polymer solar cells with P3HT:[60]PCBM, P3HT:[70]PCBM, and P3HT:bis[60]PCBM blend films deposited by inkjet printing of CB, DCB, and their mixture (1:4, 1:1, and 4:1)

Solvent	Acceptor	η (%)	FF (%)	J_{sc} (mA/cm^2)	Voc (mV)
CB	bis[60]PCBM	0.31	22	1.84	763
	[70]PCBM	1.27	41	4.97	624
	[60]PCBM	0.79	31.4	3.90	642
DCB:CB 1:4	bis[60]PCBM	0.29	24	1.81	660
	[70]PCBM	0.52	25	3.33	639
	[60]PCBM	0.85	22	6.07	629
DCB:CB 1:1	bis[60]PCBM	0.38	21	2.52	715
	[70]PCBM	0.99	26	5.98	641
	[60]PCBM	1.27	32	6.25	642
DCB:CB 4:1	bis[60]PCBM	0.74	24	4.29	740
	[70]PCBM	1.24	30	6.91	609
	[60]PCBM	2.22	38	9.49	609
DCB	bis[60]PCBM	0.21	20	2.11	516
	[70]PCBM	0.78	28	4.61	598
	[60]PCBM	0.92	29	5.33	595

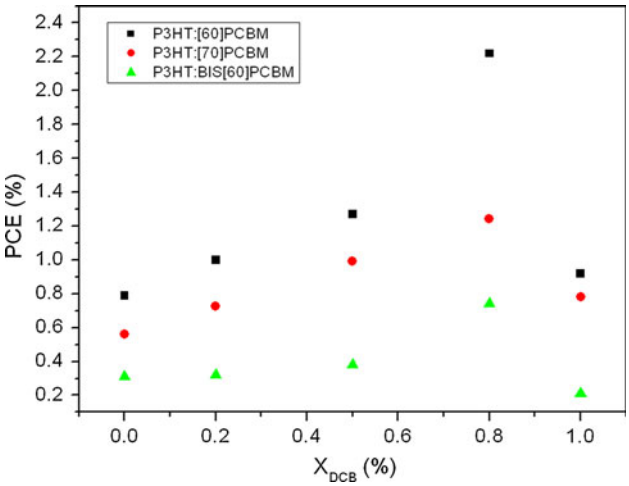

Fig. 4 PCE versus volume fraction of DCB for P3HT:[60]PCBM, P3HT:[70]PCBM, and P3HT:bis[60]PCBM blend films

for an efficient exciton dissociation the relative position of donor LUMO and acceptor LUMO is also crucial [45, 46]. Therefore, an higher LUMO level of bis[60]PCBM compared with the monoadduct justifies the higher V_{oc} value. Nevertheless, the performances of all the devices based on P3HT:bis[60]PCBM are quite poor. As shown by the AFM images, the morphology of the P3HT:bis[60]PCBM film is not optimal compared to that of P3HT:[60]PCBM and therefore needs to be further improved to achieve better performances of the corresponding devices.

Conclusion

In this study, BHJ PSCs were realized with the inkjet-printed photoactive layer by means of blend inks dissolved in different solvents (or their mixture) with different boiling points. In printed photovoltaics, the solvent composition has a key role to achieve an intimate morphology within the blend, to provide the proper spreading and wetting of the printed droplet on the underlayer and to control the droplet drying rate and the solute diffusion within the sessile drop during the drying process. All these issues influence the blend film morphology which is a crucial parameter for fabricating efficient photovoltaic devices. In this respect, PSCs were fabricated with structure glass/ITO/PEDOT:PSS/blend/Ca/Al where three different blends, P3HT:[60]PCBM, P3HT:[70]PCBM and P3HT:bis[60]PCBM, were printed from single-solvent solutions, CB and DCB, and solvent mixture solutions, DCB:CB at different volume mixing ratios. The performances of the devices were compared, to investigate the relationship between the microstructural properties of the active compounds and their efficiency in PSCs.

For the three acceptor blends, the devices fabricated from inks formulated with the solvent mixture DCB:CB 4:1 showed the highest PCE values. This result was in agreement with the best inkjet formulation generally based on the use of co-solvent systems composed by higher- and lower-boiling solvents for reaching an optimized uniformity of the printed layers. Moreover, this outcome was supported by Raman analysis which indicated for this solvent composition an higher degree molecular order of P3HT and an increase of the degree of phase separation between P3HT and PCBM. In addition, morphologic investigations by AFM revealed a good intermixing of the polymer and fullerene components. Indeed, smooth, thin films were obtained containing only few, very small nanoaggregates, which are related to the solubility of the P3HT polymer and fullerene derivatives in the used solvent system. Specifically, the optimized evaporation of this solvent mixture leads to a surface morphology of the P3HT:[60]PCBM blend having nicely defined features.

The worst performances of both the devices, P3HT:[70]PCBM and P3HT:bis[60]PCBM, can be due to an nonoptimized uniformity and morphology of the active layer. This indicates that each P3HT:fullerene blend requires an individual investigation to obtain the best properties for its optimized use in organic solar cells.

Acknowledgements The research is supported by the Italian Ministry of Economic Development within the framework of the Operating Agreement with ENEA for the Research on the Electric System.

References

1. Brabec CJ, Dyakonov V, Parisi J, Sariciftci NS (2003) Organic photovoltaics: concepts and realization, vol 60. Springer, Berlin
2. Günes S, Neugebauer H, Sariciftci NS (2007) Chem Rev 107:1324
3. Krebs FC (2009) Sol Energy Mater Sol Cells 93:394
4. Krebs FC, Spanggard H, Kjær T, Biancardo M, Alstrup J (2007) Mater Sci Eng B 138:106
5. Dennler G, Scharber MC, Brabec CJ (2009) Adv Mater 21:1323
6. Halls JJM, Friend RH (1997) Synth Met 85:130711
7. Markov DE, Amsterdam E, Blom PWM, Sieval AB, Hummelen JC (2005) J Phys Chem A 109:5266
8. Markov DE, Tanase C, Blom PWM, Wildeman J (2005) Phys Rev B 72:045217(1)
9. Yu G, Heeger AJ (1995) J Appl Phys 78:4510
10. Yu G, Gao J, Hummelen JC, Wudl F, Heeger AJ (1995) Science 270:1789
11. Tada K, Hosada K, Hirohata M, Hidayat R, Kawai T, Onoda M, Teraguchi M, Masuda T, Zakhidov AA, Yoshino K (1997) Synth Met 85:1305
12. Søndergaard R, Hösel M, Angmo D, Larsen-Olsen TT, Krebs FC (2012) Mater Today 15:36
13. Alstrup J, Jørgensen M, Medford AJ, Krebs FC (2010) ACS Appl Mater Interfaces 2:2819
14. Krebs FC, Tromholt T, Jørgensen M (2010) Nanoscale 2:873
15. Ding JM, AdlF Vornbrock, Ting C, Subramanian V (2009) Solar Energy Mater Sol Cell 93:459
16. Hoth CN, Choulis SA, Schilinsky P, Brabec CJ (2007) Adv Mater 19:3973
17. Hoth CN, Schilinsky P, Choulis SA, Brabec CJ (2008) Nano Lett 8:2806
18. Aernouts T, Aleksandrov T, Girotto C, Genoe J, Poortmans J (2008) Appl Phys Lett 92:033306(01)
19. Lange A, Wegener M, Boeffel C, Fischer B, Wedel A, Neher D (2010) Sol Energy Mater Sol Cells 94:1816
20. Eom SH, Park H, Mujawar SH, Yoon SC, Kim S–S, Na S-I, Kang S-J, Khim D, Kim D-Y, Lee S-H (2010) Org Electron 11:1516
21. Jensen J, Dam HF, Reynolds JR, Dyer AL, Krebs FC (2012) J Polym Sci B Polym Phys 50:536
22. Krebs FC, Fyenbo J, Tanenbaum DM, Gevorgyan SA, Andriessen R, van Remoortere B, Galagan Y, Jørgensen M (2011) Energy Environ Sci 4:4116
23. Krebs FC, Nielsen TD, Fyenbo J, Wadstrøm M, Pedersen MS (2010) Energy Environ Sci 3:512
24. Deegan RD (2000) Phys Rev E 61:475
25. Hu H, Larson RG (2006) J Phys Chem B 110:7090
26. Lim JA, Lee WH, Lee HS, Lee JH, Park YD, Cho K (2008) Adv Funct Mater 18:229
27. Kim D, Jeong S, Lee SH, Moon J, Song JK (2009) Synth Met 159:1381

28. Grimaldi IA, Barra M, De Girolamo Del Mauro A, Loffredo F, Cassinese A, Villani F, Minarini C (2012) Synth Met 161:2618
29. Yusli M, Way Yun T, Sulaiman K (2009) Mater Lett 63:2691
30. Tang H, Lu G, Li L, Li J, Wang Y, Yang X (2010) J Mater Chem 20:683
31. Reisdorffer F, Haas O, Le Rendu P, Nguyen TP (2012) Synth Met 161:2544
32. Zhao G, He Y, Li Y (2010) Adv Mater 22:4355
33. Chang C-Y, Wu C-E, Chen S-Y, Cui C, Cheng Y-J, Hsu C-S, Wang Y-L, Li Y (2011) Angew Chem Int Ed 50:9386
34. Wienk MM, Kroon JM, Verhees WJH, Knol J, Hummelen JC, van Hal PA, Janssen RAJ (2003) Angew Chem Int Ed 42:3371
35. Yamanari T, Taima T, Sakai J, Saito K (2008) Jpn J Appl Phys 47:1230
36. Lenes M, Wetzelaer G-JAH, Kooistra FB, Veenstra SC, Hummelen JC, Blom PWM (2008) Adv Mater 20:2116
37. Brown PJ, Thomas DS, Kőhler A, Wilson JS, Kim J-S, Ramsdale CM, Sirringhaus H, Friend RH (2003) Phys Rev B 67:064203(1)
38. Louarn G, Trznadel M, Buisson JP, Laska J, Pron A, Lapkowski M, Lefrant SJ (1996) Phys Chem 100:12532
39. Baibirac M, Lapkowski M, Pron A, Lefrant S, Baltog I (1998) J Raman Spectrosc 29:825
40. Yun J-J, Peet J, Cho N-S, Bazan GC, Lee SJ, Moskovits M (2008) Appl Phys Lett 92:251912(1)
41. Wing CT, James DT, Kim JS, Nicholson PG, Murphy CE, Bradley DDC, Nelson J, Kim J-S (2011) J Am Chem Soc 133:9834
42. Troshin PA, Hoppe H, Renz J, Egginger M, Mayorova JY, Goryachev AE, Peregudov AS, Lyubovskaya RN, Gobsch G, Sariciftci NS, Razumov VF (2009) Adv Funct Mater 19:779
43. Morvillo P, Bobeico E (2008) Sol Energy Mater Sol Cells 92:1192
44. Scharber MC, Mühlbacher D, Koppe M, Denk P, Waldauf C, Heeger AJ, Brabec CJ (2006) Adv Mater 18:789
45. Halls JJM, Cornil J, dos Santos DA, Silbey R, Hwang D-H, Holmes AB, Brédas JL, Friend RH (1999) Phys Rev B 60:5721
46. Brabec CJ, Winder C, Sariciftci NS, Hummelen JC, Dhanabalan A, van Hal PA, Janssen RAJ (2002) Adv Funct Mater 12:709